Probiotic fermentation modifies the structure of pectic polysaccharides from carrot pulp

Yujun Wan[a, b, #], Tao Hong[a, #], Huifang Shi [a], Junyi Yin[a], Todor Koev[c], Shaoping Nie[a], Robert G. Gilbert[b, d], Mingyong Xie[a*]

[a] *State Key Laboratory of Food Science and Technology, China−Canada Joint Lab of Food Science and Technology (Nanchang), Nanchang University, 235 Nanjing East Road, Nanchang, Jiangxi 330047, People's Republic of China*

[b] *Centre for Nutrition and Food Sciences, Queensland Alliance for Agriculture and Food Innovation, The University of Queensland, Brisbane, Queensland, 4072, Australia*

[c] *Food, Innovation and Health, Quadram Institute Bioscience, Norwich Research Park, Norwich NR4 7UQ, U.K.*

[d] *Joint International Research Laboratory of Agriculture and Agri-Product Safety, College of Agriculture, Yangzhou University, Yangzhou, Jiangsu 225009, China*

[#] Equal contribution

[*] Corresponding author. myxie@ncu.edu.cn (M.Y. Xie)

ABSTRACT:

Polysaccharides from fermented carrot pulp (WSP-p) show better anti-diabetic effects than those from un-fermented carrot pulp (WSP-n), and functional properties of polysaccharides depend on their structure. In this study, both WSP-p and WSP-n were separated into three homogeneous fractions as WSP-p-1, WSP-p-2, WSP-p-3, WSP-n-1, WSP-n-2 and WSP-n-3. The weight-average molecular weight of all of fractions from WSP-p showed a downward trend compared with the corresponding fraction from WSP-n. The functional groups in WSP-p and WSP-n were similar. The morphologies of WSP-p-2 and WSP-p-3 from SEM were similar to those of WSP-n-2 and WSP-n-3, but there were more fragmented particles adhered to WSP-n-1 than to WSP-p-1. Monosaccharide composition and methylation analysis confirmed that WSP-p-1, WSP-p-2, WSP-n-1 and WSP-n-2 were typical rhamnogalacturonan I-type polysaccharides with 1,4-linked α-D-galacturonic acid residues, but WSP-p-3 and WSP-n-3 contained predominantly homogalacturonan regions with 1,4-Gal*p*A linkages. ^{1}H and ^{13}C NMR of fractions from WSP-p showed the similar spectra to those from WSP-n. These findings suggest that probiotic fermentation mainly cleaved the linkages between repeating units within polysaccharides during fermentation, and not only reduced their molecular weight but also improved the homogeneity in their molecular size distribution, which improves their biofunctions.

KEYWORDS: probiotics fermentation, purification, structure, pectic polysaccharides, carrot

1. INTRODUCTION

Polysaccharides are widely found in plants, animals and microorganisms, and have a range of biological functions. They have useful bioactivities *in vivo* and *in vitro*, such as functioning as antidiabetic (Zhao et al., 2018), immune modulation (Baien et al., 2019) and anticancer agents (Ying Wang et al., 2020). Their functional activities depend upon their structure. For example, the triple helical β-glucan from *Lentinus edodes* with lower molecular weight and/or higher stiffness has stronger antitumor activity than the higher molecular weight and/or lower stiffness β-glucan from the same source (Zheng, Lu, Xu, & Zhang, 2017), and β-(1,4)-D-mannans with higher molecular weight (10 MDa) have a higher immunostimulatory activity than those with lower molecular weight (1.3 MDa) with the same acetylation degree (Ferreira, Passos, Madureira, Vilanova, & Coimbra, 2015).

Probiotic-fermented carrot pulp has been found to have a better anti-diabetic functionality than the non-fermented pulp, due to more effective regulation of glucose and lipid metabolism (Li et al., 2014; Li, Nie, Zhu, Xiong, & Xie, 2016). Our previous study showed that the hypoglycemic effects of both probiotic-fermented and non-fermented carrot pulp arise from its polysaccharides (Wan, Shi, et al., 2019). Polysaccharides from probiotic fermentation carrot pulp exhibited more positive effects in ameliorating symptoms in type II diabetic rats, which is ascribed to changes in structure caused by fermentation. *Lactobacillus plantarum* can modify polysaccharide structure by degrading glycans to tri- and tetra-saccharides during fermentation (Kaplan & Hutkins, 2000). Probiotics also use polysaccharides as prebiotics for growth during this process. However, these effects strongly depend on the linkage structure of these polysaccharides (Sims, Ryan, & Kim, 2014).

The aim of the present study is to compare the fine structure of water-soluble polysaccharides from probiotic-fermented and non-fermented carrot. To characterize the structures of complex polysaccharides, the first step is to purify the polysaccharides to obtain

several homogeneous fractions. Then, size exclusion chromatography equipped with multi-angle laser light scattering and differential refractive index detectors is employed to measure molecular size and weight distributions. Monosaccharide compositions are determined by high-performance anion-exchange chromatography, and information of functional groups is obtained using Fourier transform infrared spectroscopy. The morphology of the purified fractions is imaged with scanning electron microscopy. The position of linkages between monosaccharide residues is evaluated using methylation analysis. Other details are characterized with liquid-state proton NMR. The combination of the results could supply the structural basis for elucidating functional differences.

2. MATERIALS AND METHODS

2.1 Materials

Probiotics fermented carrot pulp (PFCP) and non-fermented carrot pulp (NFCP) were from Kuangda Biotech Co. (Nanchang, China) following the process reported elsewhere (Wan, Shi, et al., 2019). Dextran standards (T-10, T-50, T-80, T-150, T-500 and T-2000), monosaccharide standards (*L*-fucose (Fuc), *L*-rhamnose (Rha), *D*-arabinose (Ara), *D*-galactose (Gal), *D*-glucose (Glu), *D*-xylose (Xyl), *D*-mannose (Man), *D*-fructose (Fru), *D*-glucuronic acid (GlcA), and *D*-galacturonic acid (GalA)), sodium borodeuteride ($NaBD_4$) and deuterium oxide (D_2O) were purchased from Sigma-Aldrich Co. (St. Louis, USA). All of other reagents were of analytical grade and were used without further purification.

2.2 Preparation of polysaccharides

Water-soluble polysaccharides from PFCP and NFCP, isolated using the same extraction methods published elsewhere (Wan, Shi, et al., 2019), are denoted WSP-p and WSP-n respectively. Briefly, either NFCP or PFCP was extracted with deionized water twice at 100 °C for 2 h. The polysaccharide in the extracting solution was precipitated using ethanol at 4 °C

overnight after concentrating to half the original volume under reduced pressure. The precipitate was then redissolved in deionized water and treated with chloroform and N-butanol to remove the protein, based on the Sevag method (Staub, 1965). Finally, the liquid was dialyzed, concentrated and lyophilized to produce WSP-p and WSP-n.

2.3 Purification of WSP-p and WSP-n

An ÄKTA Purifier system (GE Healthcare Bio-sciences, USA) equipped with a HiLoad 26/60 Superdex-200 column was employed to purify the polysaccharide, and the eluent was divided into three fractions for both WSP-p and WSP-n (Wan, Shi, et al., 2019). A 500 mg sample of WSP-p or WSP-n was dissolved in distilled water containing 0.02% (w/w) NaN_3 and eluted with 0.1 M NaCl at a flow rate of 1.5 mL/min at 25 °C in the purifier system. These fractions of the eluant were collected, monitoring with the refractive index detector (RID). The elution profiles of both WSP-n and WSP-p recorded by the RID showed three overlapping elution peaks, denoted WSP-n-1, WSP-n-2, WSP-n-3, and WSP-p-1, WSP-p-2 and WSP-p-3.

2.4 Characterization of purified fractions

2.4.1 Size exclusion chromatography (SEC)

The molecular size distributions (MSDs) and weight-average molecular weights $\bar{M}_w$ of six purified fractions were obtained from the SEC data as described elsewhere (Watts, Gray-Weale, & Gilbert, 2007), using a SEC system equipped with an Ohpak SB-G guard column (50 mm × 6.0 mm I.D., 10 μm), an SB-806 HQ column (300 mm × 8.0 mm I.D., 13 μm) and an SB-804 HQ column (300 mm × 8.0 mm I.D., 10 μm) (Shodex Denko America, USA) in series, a refractive index detector (Wyatt, USA) and a multiple-angle laser light scattering detector (MALLS) (Wyatt, USA)**,** following the procedure described elsewhere (Wan, Xu, et al., 2019). A 100 μL sample was injected into the MALLS-SEC system and eluted with the mobile phase (0.02% (w/w) NaN_3 and 0.1 M $NaNO_3$) at 35 °C with a flow rate of 0.6 mL/min.

2.4.2 Monosaccharide compositions

These purified fractions were hydrolyzed in an oil bath with 2 M H_2SO_4 at 100 °C for 4 h and then diluted by adding distilled water, before injecting into the high-performance anion exchange chromatography device (Thermo Fisher, USA) to analyze their monosaccharide compositions. The detailed separation procedure was the same as in our previous report (Wu, Liu, Wan, Huang, & Nie, 2019).

2.4.3 Fourier transform infrared (FTIR) spectroscopy

1 mg of dried purified fraction was ground with 100 mg KBr powder and pressed into pellets to analyze the functional groups using a Fourier transform infrared spectrophotometer (Thermo Fisher, USA) over the frequency range 400 to 4,000 cm^{-1}.

2.4.4 Scanning electron microscopy

All purified fractions were dissolved in deionized water to a final concentration of 1 mg/mL and then freeze-dried to obtain the dried samples. The morphology of these samples was characterized by scanning electron microscopy (SEM, JEOL, Japan) at room temperature under an acceleration voltage of 5 kV.

2.4.5 Methylation and GC-MS analysis

A slightly modified methylation method was used based on that of (Nie et al., 2011) was used to analyze the assignments of linkages in these six fractions. Briefly, the dried sample (2-3 mg) was dissolved in 2 mL of anhydrous dimethyl sulfoxide (DMSO) by sonication for 3 h and then stirred at 80 °C for 2 h, following by stirring at room temperature overnight to completely dissolve the sample. 30 mg of dried sodium hydroxide powder was added to the solution and stirred at room temperature for 3 h. To the mixture was then added 1 mL methyl iodide and the mixture stirred for another 2.5 h to enable the methylation reaction to take place. A few drops of deionized water were added to terminate the reaction and the methylated sample was extracted with 3 mL methylene chloride, followed by hydrolysis with trifluoroacetic acid and acetylation with acetic anhydride, to obtain the partially methylated alditol acetates

(PMAAs). The PMAAs were then dissolved in methylene chloride and injected into an Agilent 7890B/7000D system equipped with a SP-2330 column (Agilent, USA). The system temperature program was increased from 160 °C to 210 °C at 2 °C/min and then to 240 °C at 5 °C/min (Wang, Yin, Huang, & Nie, 2020).

2.4.6 Nuclear magnetic resonance (NMR) spectroscopy

The six fractions were dissolved in D_2O, then lyophilized using a freezer dryer; this was repeated three times to completely remove the exchanged protons. After that, these samples were dissolved in D_2O at room temperature to conduct the NMR experiments. The ^{1}H spectra and ^{13}C spectra were obtained at 313 K with a Bruker Avance 600 MHz NMR spectrometer (Bruker, Germany).

^{1}H spectra were obtained using the integrated zg30 pulse program, with a 30° flip angle of 10.0 μs and recycle delay of 1.0 s, 64 scans and 2 dummy scans, whereas ^{13}C spectra were obtained using the zgpg30 pulse program with 30° flip angle of 10.0 s, recycle delay of 2.0 s and cpd2 decoupling sequence, 65000 scans and 4 dummy scans. ^{1}H-^{1}H nuclear Overhauser effect spectroscopy (nOeSY) experiments were performed using the noesygpph pulse sequence, where the acquisition parameters were 90° flip angle of 10.0 μs, gradient pulses of 0.2 ms, mixing time of 0.3 s, recycle delay of 2 s, 32 scans and 32 dummy scans. ^{1}H-^{1}H correlation spectroscopy (COSY) experiments were performed using the cosygpmfqf pulse sequence, with acquisition parameters of 90° flip angle of 10.0 μs, gradient pulse of 1000 μs, incremental delay of 3.0 μs, gradient recovery delay of 0.2 ms, recycle delay of 2.0 s, 128 scans and 16 dummy scans. ^{1}H-^{13}C heteronuclear single quantum correlation (HSQC) spectroscopy experiments were performed using the integrated hsqcetgp pulse sequence, with acquisition parameters of 90° flip angle of 10.0 μs, trim pulse of 1.0 ms, gradient recover delay of 0.2 ms, recycle delay of 1.5 s, 64 scans and 16 dummy scans. ^{1}H-^{13}C heteronuclear multiple bond correlation (HMBC) spectroscopy experiments were obtained using the hmbcgpndqf pulse sequence, with

acquisition parameters of ^{13}C 90° flip angle of 10.0 μs, ^{13}C 180° flip angle of 20.0 μs, ^{1}H 90° flip angle of 10.0 μs, gradient pulse of 1.0 ms, gradient recovery delay of 0.2 ms, recycle delay of 1.5 s, 128 scans and 16 dummy scans.

3. Results and discussion

SEC elution curves (Fig. 1A) from the ÄKTA Purifier system showed that both WSP-n and WSP-p were triplets, denoted WSP-n-1, WSP-n-2, WSP-n-3, WSP-p-1, WSP-p-2 and WSP-p-3, respectively. The yield of these six fractions was 15.20% (WSP-n-1), 5.16% (WSP-n-2), 16.58% (WSP-n-3), 13.42% (WSP-p-1), 2.50% (WSP-p-2) and 19.10% (WSP-p-3). The data from SEC (Fig. 1B) also confirmed that there were three components in the molecular size from the SEC results (Fig. 1C and 1D), since there was only one molecular size distribution to each fraction. The SEC results also showed that the $\overline{M}_w$ for each fraction from WSP-p was lower than the corresponding fractions in WSP-n, and this implied that probiotics used these polysaccharides to promote the growth since these polysaccharides could serve as potential prebiotics (P. Chen et al., 2019).

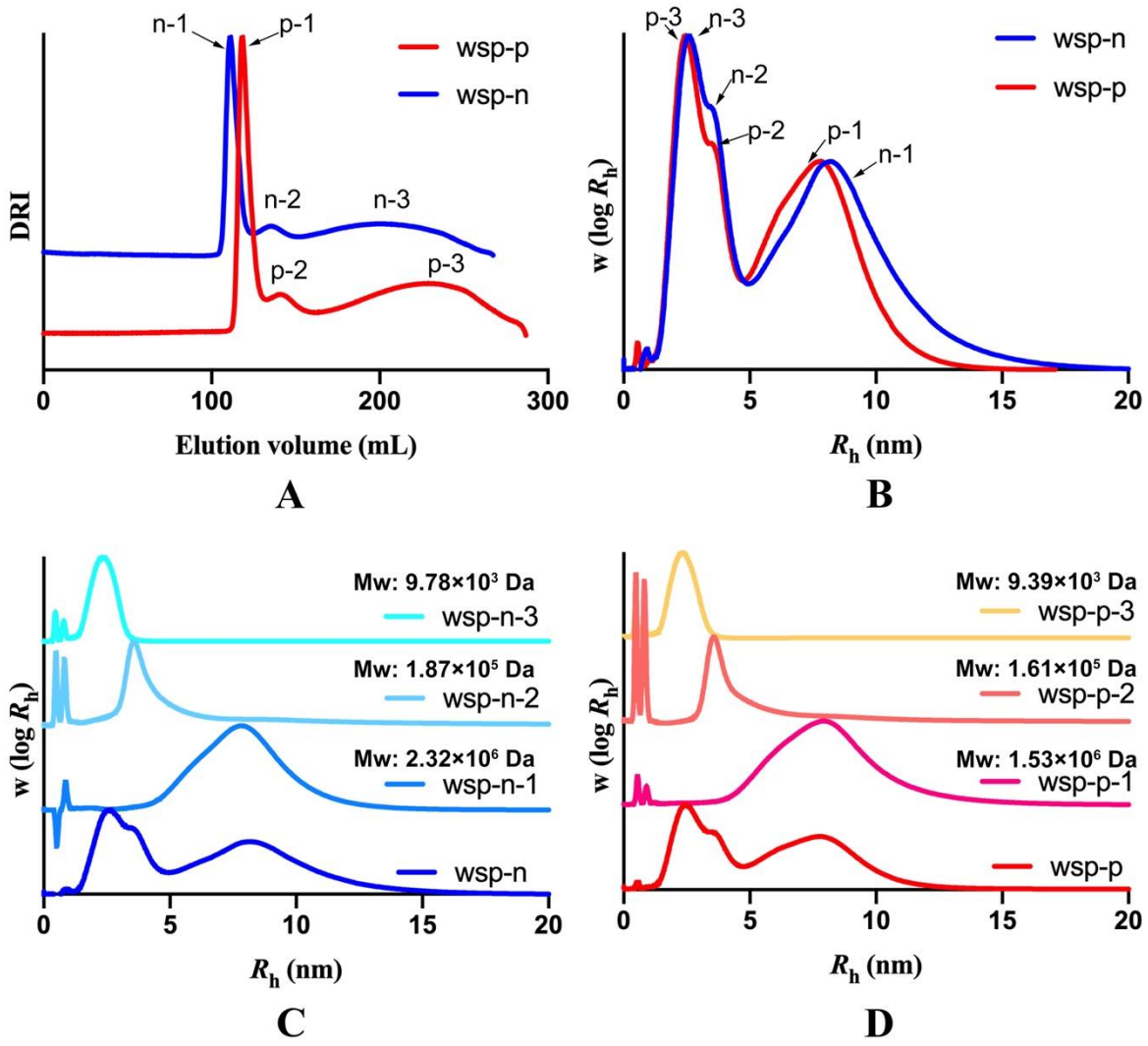

Figure 1. Elution curves and molecular size distributions (MSDs) (A. Elution curves of wsp-p and wsp-n; B. MSDs of wsp-p and wsp-n; C. MSDs of wsp-n-1, wsp-n-2 and wsp-n-3; D. MSDs of wsp-p-1, wsp-p-2 and wsp-p-3)

3.2 Monosaccharide compositions

Table 1 shows that all six purified fractions were typical pectic polysaccharides, mainly containing Rha, Ara, Gal and GalA as their monomer units. Glucose may originate from the non-pectic polysaccharides, such as cellulose and hemicellulose (Deng et al., 2020). Neutral sugars predominated in WSP-n-1, WSP-n-2, WSP-p-1 and WSP-p-2 (> 85% in all four fractions). By contrast, there were more than 70% uronic acid units within both WSP-n-3 and WSP-p-3. GalA is the main monomer unit of homogalacturonan (HG) and rhamnogalacturonan (RG) (Deng et al., 2020). Table 1 shows that all of these six fractions had the RG and HG

domain within their structure. The molar components of the RG-I and HG domains have been estimated as follows: RG-I = (GalA – HG) + Rha +Ara + Gal, HG = GalA – Rha (E. G. Shakhmatov, Toukach, Michailowa, & Makarova, 2014). RG-I was the predominant component in both fractions 1 and 2. The HG domains within WSP-n-1 and WSP-n-2 decreased after fermentation, but their RG-I domains increased. HG was the main constituent within fraction 3, being higher than 60% in both of WSP-n-2 and WSP-p-2.

Table 1. Chemical compositions of purified fractions [α]

	Rha (%)	Ara (%)	Gal (%)	Glc (%)	GalA (%)
WSP-n-1	6.45 ± 1.05[a]	32.87 ± 1.11[a]	49.01 ± 1.23[a]	1.12 ± 0.07[a]	10.55 ± 0.89[a]
WSP-p-1	8.80 ± 0.61[b]	30.75 ± 0.64[a]	47.68 ± 1.54[a]	0.95 ± 0.06[a]	11.82 ± 0.10[a]
WSP-n-2	4.57 ± 0.27[a]	33.85 ± 0.32[a]	45.93 ± 0.40[a]	3.30 ± 0.79[a]	12.30 ± 1.20[a]
WSP-p-2	5.88 ± 0.23[a]	35.05 ± 0.75[b]	46.26 ± 0.60[b]	1.06 ± 0.05[a]	11.75 ± 0.65[a]
WSP-n-3	5.39 ± 0.03[a]	7.61 ± 0.02[a]	7.70 ± 0.04[a]	8.82 ± 0.24[a]	70.53 ± 0.16[a]
WSP-p-3	4.72 ± 0.06[a]	9.55 ± 0.05[b]	9.55 ± 0.02[b]	3.23 ± 0.06[b]	73.98 ± 0.76[b]

[α] Different letters represent significant differences ($p < 0.05$)

3.3 FTIR

Fig. 2 shows the FTIR spectra of the six purified fractions. An absorption at around 3400 cm^{-1} is attributed to the hydroxyl group, the band at approximately 2930 cm^{-1} to a C-H stretch, that at about 1640 cm^{-1} to a carboxylate group near 1750 cm^{-1} to esterified carboxyl groups; this last also overlaps with the free carboxyl group. It is seen that each of the purified fractions (WSP-n-1, WSP-n-2 and WSP-n-3) contains the same functional groups as the corresponding fractionsin WSP-p. This result indicated that probiotics fermentation did not change the functional group of polysaccharides from carrot.

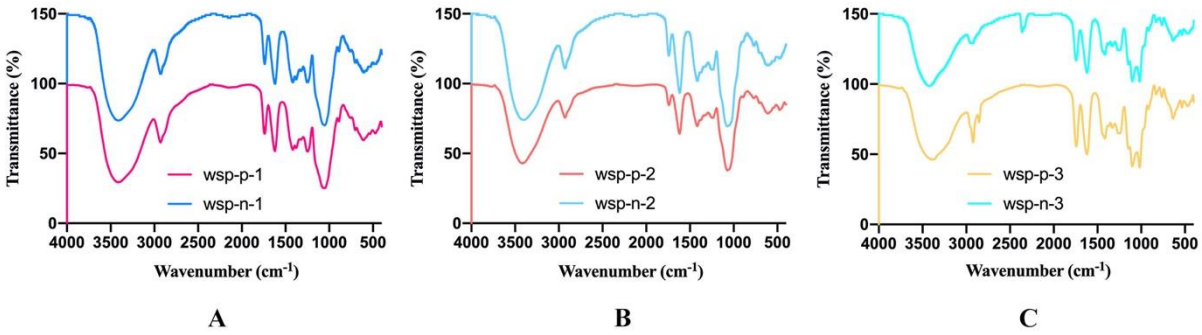

206

207 **Figure 2.** FTIR spectra of purified fractions

208 3.4 SEM

209 Fig. 3 compares the SEM micrographs of these six different purified fractions. All of these
210 samples had multi-layer arrangements and showed highly inter-connected networks. There was
211 an obvious difference between WSP-n-1 and WSP-p-1. While the morphology of WSP-n-1
212 showed many fragmented particles adhering to large particles, that of WSP-p-1 only had large
213 particles with smooth surfaces. Both images of WSP-n-2 and WSP-p-2 showed similar rough
214 surfaces, but WSP-n-3 and WSP-p-3 had smoother surfaces. These results suggest that there
215 still were some minor changes in their structural features, since the morphologies of WSP-p-1
216 and WSP-n-1 showed some differences, and the morphology difference represented the
217 difference in their structure (Qi et al., 2020).

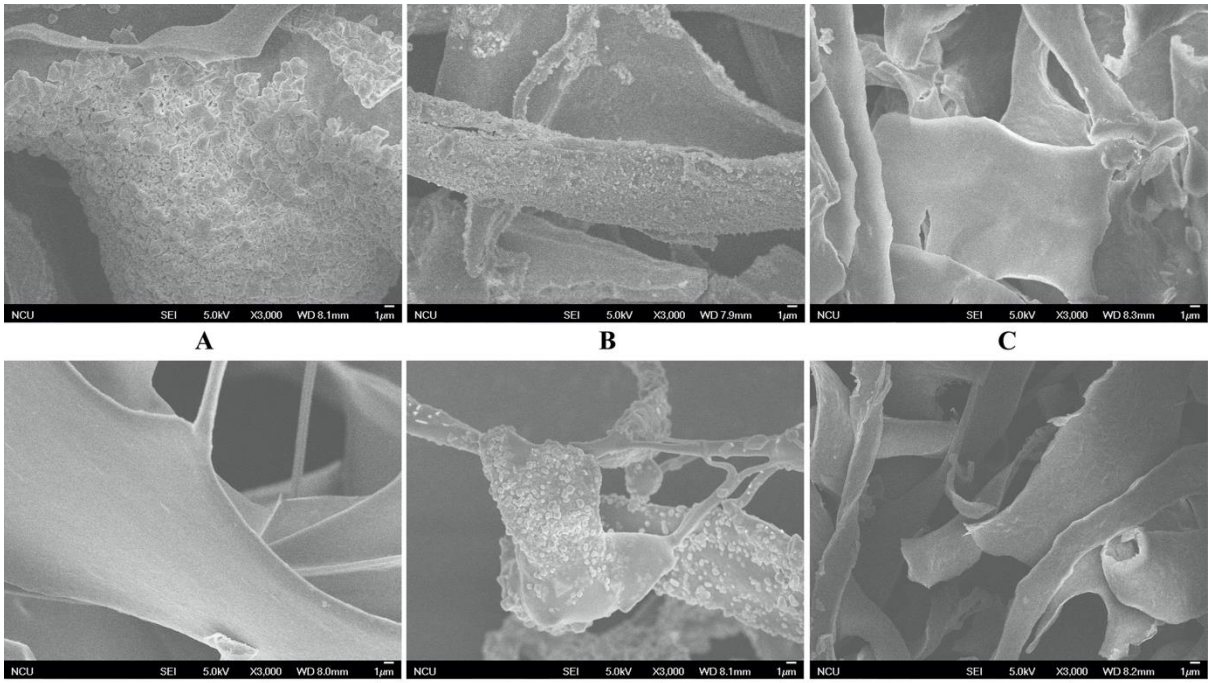

Figure 3. SEM micrographs of different purified fractions (A. WSP-n-1, B. S WSP-n-2, C. WSP-n-3, D. WSP-p-1, E. WSP-p-2 and F. WSP-p-3)

3.5 Linkages pattern

Results from methylation analysis of the reduced WSP-n-1 and WSP-p-1 are shown in Table 2. The fermentation process did not noticeably change the linkage patterns of fraction 1 purified from carrot polysaccharide because the glycosidic bonds types of WSP-n-1 and WSP-p-1 remained basically the same. Results from the GC-MS showed that the glycosidic bonds types of these two polysaccharides were similar. However, there are some differences in the molar ratio of their glycosidic bonds. The structure of fraction 1 (both WSP-n-1 and WSP-p-1) was complex, with nearly 20 types of linkage patterns, in which 1,4-Gal*p*, 1,5-Ara*f* and T-Ara*f* residues were the main residues. Additionally, the presence of 1,2,4-Rha*p*, 1,3,5-Ara*f*, T-Gal*p*, 1,4-Gal*p*A and 1,4,6-Gal*p* residues were detected. The results of linkage pattern analysis of WSP-n-1 and WSP-p-1 indicated that fraction 1 was a typical RG-I type pectin, which is was consistent with the results of monosaccharide composition analysis (Atmodjo, Hao, & Mohnen, 2013; Cardoso, Ferreira, Mafra, Silva, & Coimbra, 2007). The main glycosidic linkage types

in WSP-n-2 and WSP-p-2 were similar to fraction 1, including T-Ara*f*, 1,5-Ara*f* and 1,4-Gal*p* residues (Table 2). Because of the relatively small amount of sample, fraction 2 had to be subjected to methylation analysis without reduction; thus, information on uronic acid could not be obtained, and the presence of rhamnose could not be detected (Pettolino, Walsh, Fincher, & Bacic, 2012).

As shown in Table 2, the dominant sugar residue in WSP-n-3 and WSP-p-3 was 1,4-Gal*p*A, accounting for more than 60 mol% of all the sugar residues, which is in accordance with the result of monosaccharide composition analysis, that fraction 3 is mainly composed of GalA. This indicated that WSP-n-3 and WSP-p-3 were typical HG-type pectic polysaccharides (Evgeny G Shakhmatov, Toukach, & Makarova, 2020), and there were no changes in linkage pattern of these fractions, and only minor difference in their molar ratio of each linkage pattern.

Table 2. Linkage analysis of different purified fractions (mol%) [a]

Linkage pattern	WSP-n-1	WSP-p-1	WSP-n-2	WSP-p-2	WSP-n-3	WSP-p-3
T-Ara*f*	16.63	14.28	31.94	31.68	2.19	4.68
1,2-Rha*p*	2.15	3.27	n.d.	n.d.	n.d.	n.d.
T-Gal*p*	5.02	5.90	2.95	2.67	8.59	11.90
1,5-Ara*f*	11.59	12.56	20.71	20.44	4.64	2.65
1,2,4-Rha*p*	6.06	7.16	n.d.	n.d.	n.d.	n.d.
1,3,5-Ara*f*	5.8	6.38	9.14	5.99	n.d.	n.d.
1,4-Gal*p*	29.32	24.64	22.74	17.78	1.39	1.52
1,4-GalA*p*	7.45	6.32	n.d.	n.d.	67.01	61.24
1,2,5- Ara*f*	2.48	2.76	4.12	3.14	n.d.	n.d.
1,4-Glc*p*	0.65	1.32	n.d.	n.d.	3.01	2.19
1,6-Gal*p*	1.03	1.31	1.99	6.46	1.48	2.51
1,3,4-Gal*p*	1.7	2.09	n.d.	n.d.	3.02	3.32
1,2,4-Gal*p*	2.67	2.69	n.d.	n.d.	2.01	2.19
1,2,3,4-Gal*p*	0.60	0.79	n.d.	n.d.	n.d.	n.d.
1,4,6-Gal*p*	4.76	6.00	1.98	1.02	5.86	6.64
1,3,6-Gal*p*	0.37	0.50	2.74	8.78	0.78	1.15
1,3,4,6-Gal*p*	0.76	1.08	1.69	2.06	n.d.	n.d.
1,2,4,6-Gal*p*	0.94	0.96	n.d.	n.d.	n.d.	n.d.

[a] n.d.: Not detected

3.6 NMR

The ^{13}C and ^{1}H spectra of WSP-n-1 and WSP-p-1 are presented in Figure 4. From the similarity of the NMR spectra, it seems that the fermentation process did not significantly change the structural features of fraction 1. In accordance with the complex methylation analysis results, the anomeric proton and carbon region of WSP-n-1 and WSP-p-1 were relatively complicated. This was in accordance with all 2D NMR spectra, where the difference in chemical shift and cross-peak position varied minimally between WSP-n-1 and WSP-p-1 fractions. The resonances at δ 4.54/104.08 ppm and 4.56/103.41 ppm corresponded to the

anomeric proton and carbon of β-1,4-Gal*p* and β-T-Gal*p*, respectively. For arabinose residues, signals at δ 5.06/106.66 ppm and 5.00/107.08 ppm are assigned to α-T-Ara*f* and α-1,5- Ara*f* (Dias, Barbieri, Fetzer, Corazza, & Silveira, 2020; Rakhmanberdyeva, Zhauynbayeva, Senchenkova, Shashkov, & Bobakulov, 2019). The small peaks at high field, δ 1.22 ppm in the ^{1}H spectrum and 16.54 ppm in the ^{13}C spectrum, are assigned to the CH_3 (C6) of rhamnose, demonstrating the presence of this sugar residue. The anomeric proton and carbon of rhamnose are assigned to δ 4.89/97.67 ppm. The signals present at low field, δ 175–170 ppm, in the ^{13}C spectrum are assigned to the carboxyl carbons of Gal*p*A, indicating the presence of uronic acid and methyl-esterified uronic acid, which is consistent with the monosaccharide composition results (Patova et al., 2019).

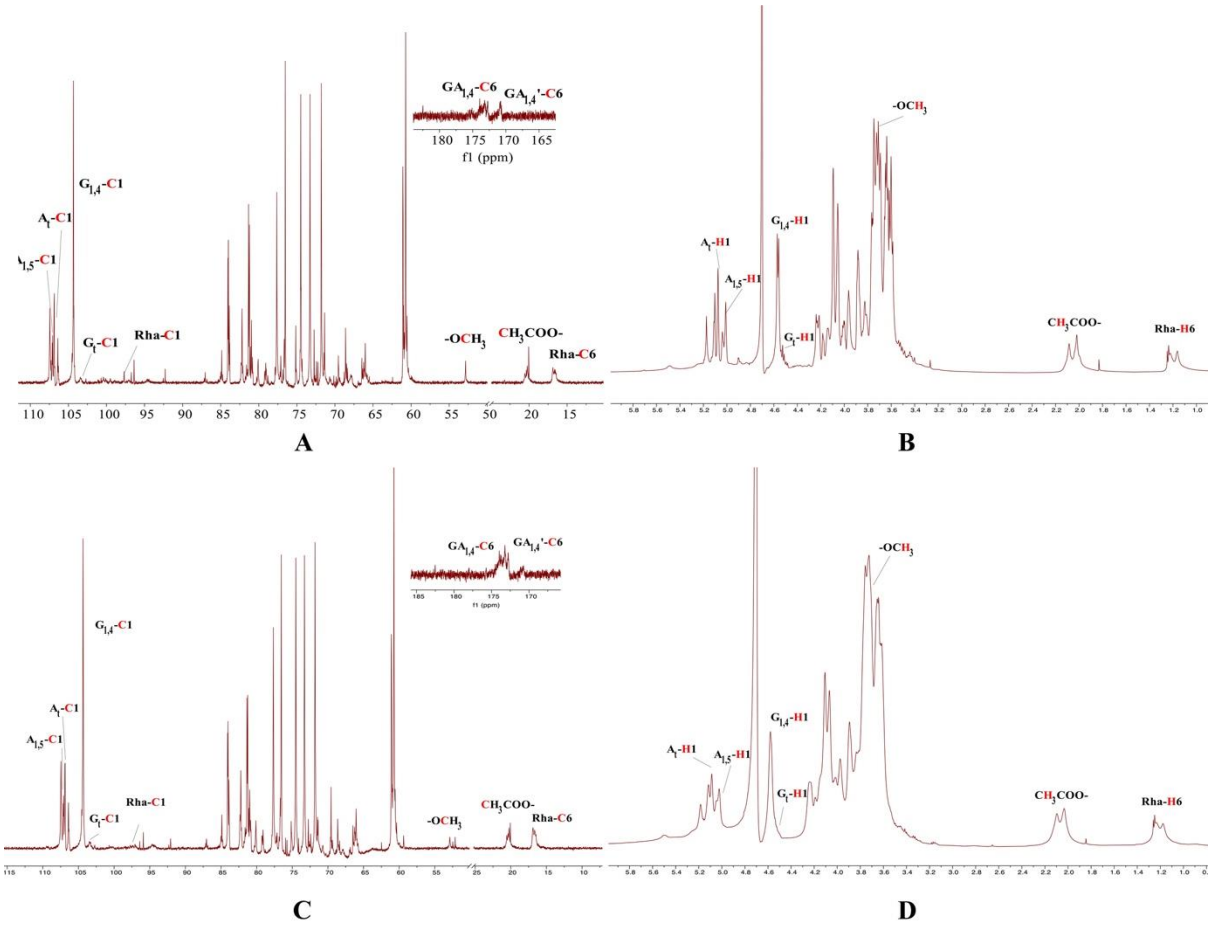

Figure 4. ^{13}C NMR spectra of WSP-n-1 (a) and WSP-p-1 (c); ^{1}H NMR of WSP-n-1 (b) and WSP-p-1 (d). GA: Gal*p*A.

Because of the relatively small amount of sample, the quality of the NMR spectra of WSP-n-2 and WSP-p-2 are not ideal. However, the signals of this fraction are similar to those of fraction 1, mainly containing peaks of β-1,4-Gal*p*, β-T-Gal*p*, α-T-Ara*f* and α-1,5-Ara*f*, indicating the compositional similarity of fraction 1 and 2.

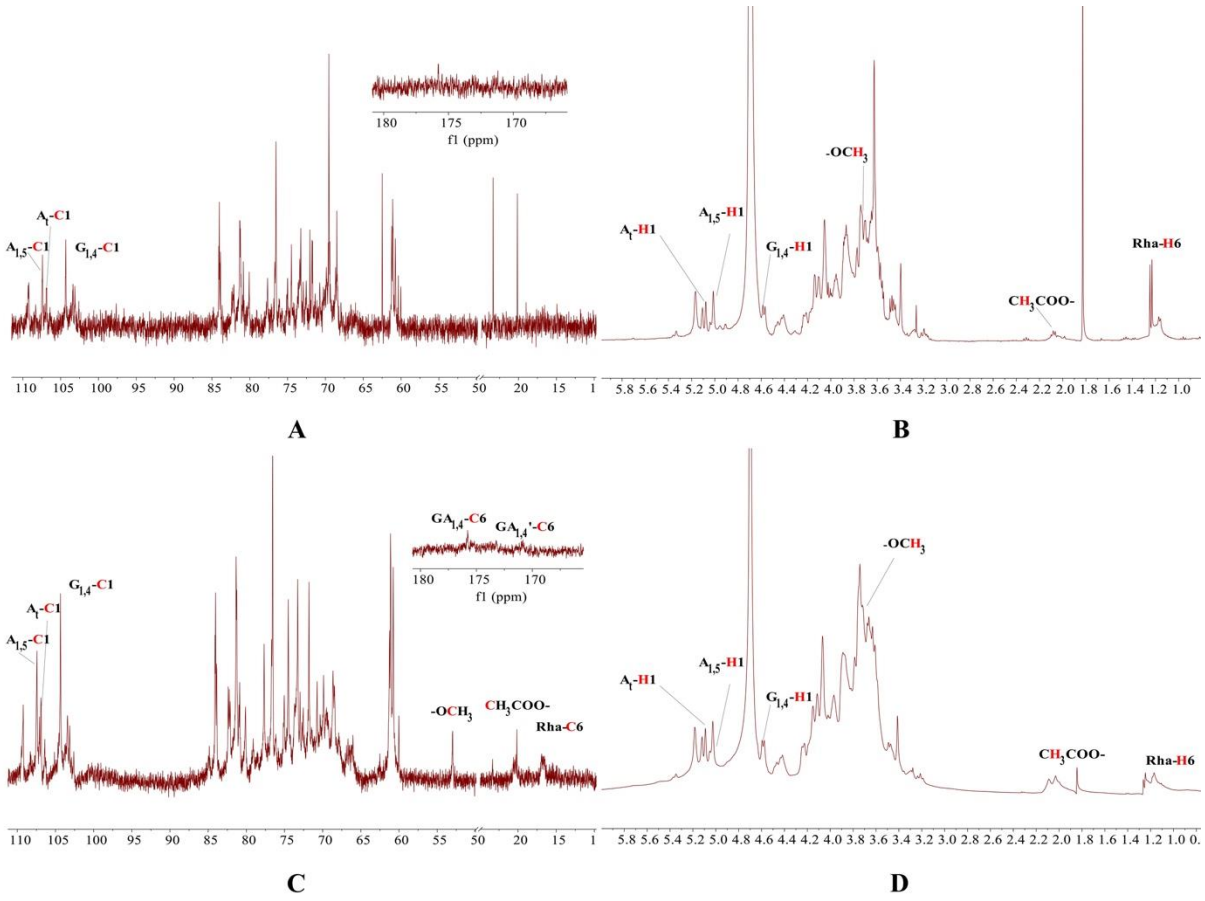

Figure 5. ^{13}C NMR of WSP-n-2 (a) and WSP-p-2 (c); ^{1}H NMR of WSP-n-2 (b) and WSP-p-2 (d). GA: Gal*p*A; GA': Gal*p*A(OMe) ; G: Gal*p*; A: Ara.

The results also suggest that the probiotic fermentation process had only minor influence on the structure of carrot water-soluble polysaccharide fraction 3, where no differences were detected in the 2D spectra of the unfermented and fermented fractions. Fraction 3 was a typical HG-type polysaccharide, as confirmed by the NMR results. Signals at δ 4.87 ppm, 5.01 ppm and 5.22 ppm in the ^{1}H spectrum and δ 99.94 ppm, 99.16 ppm and 92.13 ppm in the ^{13}C spectrum are assigned to anomeric proton and carbon signals of α-1,4-Gal*p*A, methyl esterified α-1,4-Gal*p*A (Gal*p*Ame) and α-T-Gal*p*A residues, respectively. The signals at δ 175.53 ppm

and 170.87 ppm in the ^{13}C spectrum were assigned to C6 of α-1,4-Gal*p*A and methyl esterified α-1,4-Gal*p*A (Patova et al., 2019). The most intense and sharpest peak at δ 3.72 ppm in the ^{1}H spectrum and δ 52.82 ppm in the ^{13}C spectrum in Fig. 4 is attributed to the methoxy group, indicating some of the carboxyl groups of α-1,4-Gal*p*A residues were methyl esterified (Guo, Du, Jiang, Goff, & Cui, 2019). Additionally, signals at δ 2.08 ppm in the ^{1}H spectrum and δ 20.16 ppm in the ^{13}C spectrum was assigned to acetyl groups, suggesting O-acetate substitution in α-1,4-Gal*p*A residues (Patova et al., 2019).

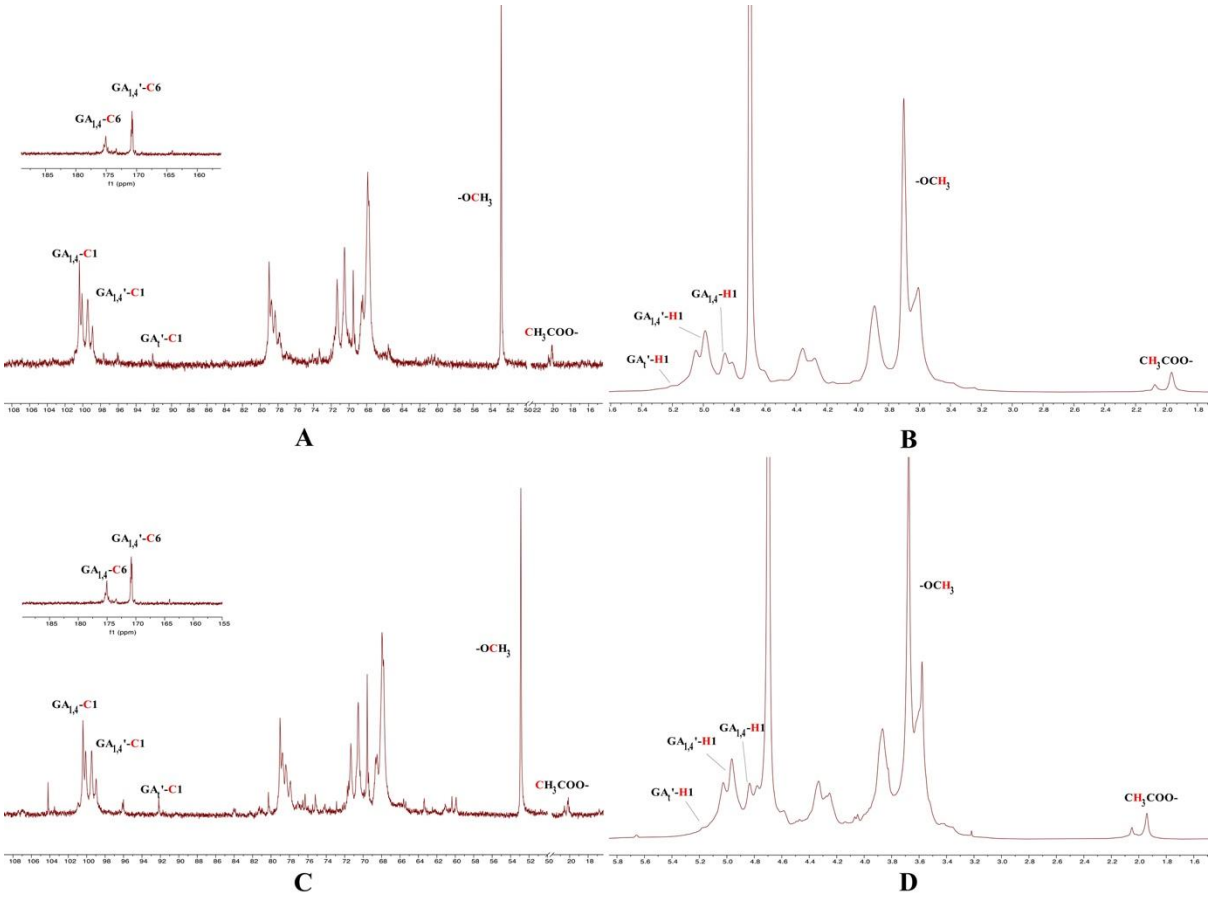

Figure 6. ^{13}C NMR of WSP-n-3 (a) and WSP-p-3 (c); ^{1}H NMR of WSP-n-3 (b) and WSP-p-3 (d). GA: Gal*p*A; GA': Gal*p*A(OMe)

4. Conclusions

The structural comparison studies of these six pectic polysaccharides provide show the effects of probiotics fermentation on structural changes of carrot polysaccharides. WSP-n-1,

WSP-n-2, WSP-p-1 and WSP-p-2 are typical RG-I pectic polysaccharides with similar structural features. However, WSP-n-3 and WSP-p-3 are predominantly HG-type pectic polysaccharides. The probiotics seem to only cleave the linkages between repeating units within these polysaccharides and then use the products to support to their growth during fermentation process (P. Chen et al., 2019). Thus, the molecular weights of these three fractions from WSP-p are lower than those from WSP-n. At the same time, because of the modification by probiotic fermentation, the purified fractions from WSP-p showed the more homogeneous molecular size distributions than the corresponding fractions from WSP-n. Since they have the same repeating units, their linkage pattern and NMR spectra show similar features. All these characterization results from these six fractions suggest that the differences in functional activities between WSP-n and WSP-p arise from differences in their fine structural features. The modified WSP (WSP-p) was the polysaccharides with the lower molecular weight and more homogeneous glycan than the original WSP (WSP). These modified polysaccharides probably have higher scavenging rates for reactive oxygen species and then may help to protect cells against impairments to blood-sugar regulation (X. Q. Chen et al., 2011; Xiao & Jiang, 2015). However, it is also should be noted that techniques to characterize the complex pectic polysaccharides are immature, since the substrates in the present study contain mainly GalA as their monomer unit. Therefore, there may be more difference between WSP-n and WSP-p, which is an area for further investigation.

Acknowledgement

This work was supported from the National Natural Science Foundation of China (31571826), the Outstanding Science and Technology Innovation Team Project in Jiangxi Province (20165BCB19001), and the Collaborative Project in Agriculture and Food Field between China and Canada (2017ZJGH0102001).

References

Atmodjo, M. A., Hao, Z., & Mohnen, D. (2013). Evolving views of pectin biosynthesis. *Annual Review Plant Biology,* 64, 747-779.

Baien, S. H., Seele, J., Henneck, T., Freibrodt, C., Szura, G., Moubasher, H., . . . Singh, M. (2019). Antimicrobial and immunomodulatory effect of Gum arabic on human and bovine granulocytes against Staphylococcus aureus and Escherichia coli. *Frontiers in Immunology,* 10, 3119.

Cardoso, S. M., Ferreira, J. A., Mafra, I., Silva, A. M., & Coimbra, M. A. (2007). Structural ripening-related changes of the arabinan-rich pectic polysaccharides from olive pulp cell walls. *Journal of Agricultural and Food Chemistry,* 55(17), 7124-7130.

Chen, P., You, Q., Li, X., Chang, Q., Zhang, Y., Zheng, B., . . . Zeng, H. (2019). Polysaccharide fractions from Fortunella margarita affect proliferation of Bifidobacterium adolescentis ATCC 15703 and undergo structural changes following fermentation. *International Journal of Biological Macromolecules,* 123, 1070-1078.

Chen, X. Q., Wang, Y. F., Wu, Y. L., Han, B. Y., Zhu, Y. J., Tang, X. L., & Sun, Q. L. (2011). Green tea polysaccharide-conjugates protect human umbilical vein endothelial cells against impairments triggered by high glucose. *International Journal of Biological Macromolecules,* 49(1), 50-54.

Deng, Z., Pan, Y., Chen, W., Chen, W., Yun, Y., Zhong, Q., . . . Chen, H. (2020). Effects of cultivar and growth region on the structural, emulsifying and rheological characteristic of mango peel pectin. *Food Hydrocolloids,* 103, 105707.

Dias, I. P., Barbieri, S. F., Fetzer, D. E. L., Corazza, M. L., & Silveira, J. L. M. (2020). Effects of pressurized hot water extraction on the yield and chemical characterization of pectins from Campomanesia xanthocarpa Berg fruits. *International Journal of Biological Macromolecules,* 146, 431-443.

Ferreira, S. S., Passos, C. P., Madureira, P., Vilanova, M., & Coimbra, M. A. (2015). Structure–function relationships of immunostimulatory polysaccharides: A review. *Carbohydrate Polymers,* 132, 378-396.

Guo, Q., Du, J., Jiang, Y., Goff, H. D., & Cui, S. W. (2019). Pectic polysaccharides from hawthorn: Physicochemical and partial structural characterization. *Food Hydrocolloids,* 90, 146-153.

Kaplan, H., & Hutkins, R. W. (2000). Fermentation of fructooligosaccharides by lactic acid bacteria and bifidobacteria. *Applied and Environmental Microbiology,* 66(6), 2682-2684.

Li, C., Ding, Q., Nie, S., Zhang, Y., Xiong, T., & Xie, M. (2014). Carrot juice fermented with Lactobacillus plantarum NCU116 ameliorates type 2 diabetes in rats. *Journal of Agricultural and Food Chemistry,* 62(49), 11884-11891.

Li, C., Nie, S., Zhu, K., Xiong, T., & Xie, M. (2016). Lactobacillus plantarum NCU116 fermented carrot juice evokes changes of metabolites in serum from type 2 diabetic rats. *Food Research International,* 80, 36-40.

Nie, S., Cui, S. W., Phillips, A. O., Xie, M., Phillips, G. O., Al-Assaf, S., & Zhang, X. (2011). Elucidation of the structure of a bioactive hydrophilic polysaccharide from Cordyceps sinensis by methylation analysis and NMR spectroscopy. *Carbohydrate Polymers,* 84(3), 894-899.

Patova, O., Smirnov, V., Golovchenko, V., Vityazev, F., Shashkov, A., & Popov, S. (2019). Structural, rheological and antioxidant properties of pectins from Equisetum arvense L. and Equisetum sylvaticum L. *Carbohydrate Polymers,* 209, 239-249.

Pettolino, F. A., Walsh, C., Fincher, G. B., & Bacic, A. (2012). Determining the polysaccharide composition of plant cell walls. *Nature Protocol*, 7(9), 1590-1607.

Qi, X. L., Su, T., Zhang, M. Y., Tong, X. Q., Pan, W. H., Zeng, Q. K., & Shen, J. L. (2020). Sustainable, flexible and biocompatible hydrogels derived from microbial polysaccharides with tailorable structures for tissue engineering. *Carbohydrate Polymers,* 237, 116160.

Rakhmanberdyeva, R., Zhauynbayeva, K., Senchenkova, S., Shashkov, A., & Bobakulov, K. M. (2019). Structure of arabinogalactan and pectin from the Silybum marianum. *Carbohydrate Research,* 485, 107797.

Shakhmatov, E. G., Toukach, P. V., & Makarova, E. N. (2020). Structural studies of the pectic polysaccharide from fruits of Punica granatum. *Carbohydrate Polymers,* 235, 115978.

Shakhmatov, E. G., Toukach, P. V., Michailowa, C., & Makarova, E. N. (2014). Structural studies of arabinan-rich pectic polysaccharides from Abies sibirica L. Biological activity of pectins of A. sibirica. *Carbohydrate Polymers,* 113, 515-524.

Sims, I. M., Ryan, J. L., & Kim, S. H. (2014). Inávitro fermentation of prebiotic oligosaccharides by Bifidobacterium lactis HN019 and Lactobacillus spp. *Anaerobe,* 25, 11-17.

Staub, A. (1965). Removeal of protein-Sevag method. *Methods in Carbohydrate Chemistry,* 5, 5-6.

Wan, Y., Shi, H., Xu, R., Yin, J., Nie, S., Xiong, T., & Xie, M. (2019). Origin of Hypoglycemic Benefits of Probiotic-Fermented Carrot Pulp. *Journal of Agricultural and Food Chemistry,* 67(3), 895-904.

Wan, Y., Xu, M., Gilbert, R. G., Yin, J., Huang, X., Xiong, T., & Xie, M. (2019). Colloid chemistry approach to understand the storage stability of fermented carrot juice. *Food Hydrocolloids,* 89, 623-630.

Wang, Y., Han, Q., Bai, F., Luo, Q., Wu, M., Song, G., . . . Wang, Y. (2020). The assembly and antitumor activity of lycium barbarum polysaccharide-platinum-based conjugates. *Journal of Inorganic Biochemistry,* 205, 1-10.

Wang, Y., Yin, J., Huang, X., & Nie, S. (2020). Structural characteristics and rheological properties of high viscous glucan from fruit body of Dictyophora rubrovolvata. *Food Hydrocolloids,* 101, 1-10.

Watts, C. J., Gray-Weale, A., & Gilbert, R. G. (2007). Interpreting size-exclusion data for highly branched biopolymers by reverse Monte Carlo simulations. *Biomacromolecules,* 8(2), 455-463.

Wu, G., Liu, D., Wan, Y., Huang, X., & Nie, S. (2019). Comparison of hypoglycemic effects of polysaccharides from four legume species. *Food Hydrocolloids,* 90, 299-304.

Xiao, J. B., & Jiang, H. X. (2015). A Review on the Structure-Function Relationship Aspect of Polysaccharides from Tea Materials. *Critical Reviews in Food Science and Nutrition,* 55(7), 930-938.

Zhao, L., Zhang, F., Ding, X., Wu, G., Lam, Y. Y., Wang, X., . . . Ma, J. (2018). Gut bacteria selectively promoted by dietary fibers alleviate type 2 diabetes. *Science,* 359(6380), 1151-1156.

Zheng, X., Lu, F., Xu, X., & Zhang, L. (2017). Extended chain conformation of β-glucan and its effect on antitumor activity. *Journal of Materials Chemistry B,* 5(28), 5623-5631.